

Vortex States of a Superconducting Film from a Magnetic Dot Array

D. J. Priour Jr¹, H. A. Fertig²

¹*Condensed Matter Theory Center, Department of Physics,
University of Maryland, College Park, MD 20742-4111*

²*Department of Physics and Astronomy, University of Kentucky, Lexington, KY 40506-0055*

Using Ginzburg-Landau theory, we find novel configurations of vortices in superconducting thin films subject to the magnetic field of a magnetic dot array, with dipole moments oriented perpendicular to the film. Sufficiently strong magnets cause the formation of vortex-antivortex pairs. In most cases, the vortices are confined to dot regions, while the antivortices can form a rich variety of lattice states. We propose an experiment in which the perpendicular component of the dot dipole moments can be tuned using an in-plane magnetic field. We show that in such an experiment the vortex-antivortex pair density shows broad plateaus as a function of the dipole strength. Many of the plateaus correspond to vortex configurations which break dot lattice symmetries. In some of these states, the vortex cores are strongly distorted. Possible experimental consequences are mentioned.

PACS numbers: PACS numbers: 74.20.-z, 74.25.Qt, 74.78.-w, 68.55.Ln, 68.65.Cd, 61.46.+w

Type II superconductors, with their high critical currents and fields, lend themselves to technological applications. However, vortices appear in these superconducting systems when magnetic fields or currents are made sufficiently large. Motion of the vortices spoils the perfect conductivity important in applications; it is therefore important to find ways to pin flux quanta. Systematic studies of vortex pinning have been carried out in experiments on regular nanoscale arrays where a lattice of defects is superimposed on a thin superconducting film. “Antidot” arrays, in which pinning centers consist of holes or depressions in the substrate, were first to be studied [1]. Subsequently, magnetic dot arrays have been created, usually by the deposition of mesoscopic magnetic dipoles on top of the superconducting film [2–7]. In the case of the nanoscale magnetic dot arrays, a number of experimental and theoretical studies have focused on scenarios in which each unit cell is penetrated by a finite amount of net magnetic flux. In this work, we consider arrays of dipoles for which there is no net perpendicular applied field. Even without any applied net flux, we show that rich vortex phenomena occur as one changes the strength of the dot dipoles. We propose an experimental scenario to observe these effects, in which an in-plane applied magnetic field is used to tilt the dipole moments. The thin film geometry prevents the horizontally directed field from disturbing the superconducting state, and tilting the moments makes possible the adjustment of the effective strength of the magnetic dots.

In our work, we focus on the case in which the dipoles prefer an orientation perpendicular to the superconducting film. The supercurrents which the magnetic dots induce move in a clockwise direction. The resulting cancellation of the field from the array magnets is a partial realization of the Meissner effect. With the induced currents, there is an associated cost in kinetic energy; hence, for sufficiently strong dipoles, it is energetically favorable to have a vortex in the vicinity of the dot, since this al-

lows the vortex’s counterclockwise currents to partially cancel the induced currents. However, due to the zero flux condition, vortices cannot form in isolation; vortices and antivortices must be generated in pairs.

Some work has concentrated on isolated magnets, where the entire system has cylindrical symmetry [8–11]. A few studies in the framework of the London theory have focused on a single pair of flux quanta in one unit cell, using periodic boundary conditions [12–17]. Depinning has been studied in the Ginzburg-Landau framework, but for antidots rather than magnetic dots [18]. Because vortices must be put in by hand in the London theory, it is not straightforward to go beyond simple situations (generally one vortex-antivortex pair in a single unit cell). However vortices appear naturally in a Ginzburg-Landau treatment, making tractable more complicated situations, such as those involving multiple flux quanta pairs in a unit cell, where often one must allow for superlattice structures. In this work, to avoid assuming the same vortex configuration for each unit cell, we study a large (4×4) supercell with periodic boundary conditions. In what follows, ρ_{pair} denotes the number of vortex-antivortex pairs per unit cell. We find that as the strength of the dot magnets is varied (by tilting dipole moments via an in-plane magnetic field), ρ_{pair} exhibits sharply defined plateaus. Remarkably, the vortex pair density is not always a monotonic function of the dipole strength. We will see that there are stable vortex states which break orientational and/or mirror symmetry. Phase transitions which can be abrupt or continuous occur as the dipole strength is varied. In the abrupt case, hysteresis phenomena are found, consistent with their being first order transitions. Surprisingly, some of these occur within a plateau. As will be discussed, second order transitions define shifts between plateaus in which ρ_{pair} either increases or decreases via the annihilation or creation of a vortex-antivortex pair. A gradual deformation of the vortex and antivortex cores is associated with the

creation or destruction of a flux quantum pair. Since London theory does not take into account variations of the Cooper pair density, and therefore cannot correctly describe vortex cores, Ginzburg-Landau theory is essential to describe these novel states.

Methods and Results— To study our system in the Ginzburg-Landau framework, we solve the nonlinear partial differential equations which one finds on extremizing the Ginzburg-Landau internal energy given by

$$E_{GL} = d\Delta\xi^3 \int \left[\left| \psi^* \left(\vec{\nabla}/i - \vec{A} \right) \psi \right|^2 - |\psi|^2 + \frac{\kappa^2}{2} |\psi|^4 + (\vec{B} - \vec{B}_{ext})^2 \right] d^3x. \quad (1)$$

In Eq. 1, dimensionless units are used; as a result, all linear dimensions are expressed in terms of the superconducting coherence length ξ . The constant Δ is the condensation energy per unit volume for a uniform bulk superconductor and the film thickness (in units of ξ) is given by d . Since $d \ll \xi$, we view the superconducting substrate as a film of negligible thickness. Hence, one would not expect an in-plane magnetic field imposed to tilt the dipole moments of the dot magnets to affect the superconducting state in the film. We assume the mesoscopic magnetic dipoles above the substrate to have a square cross section. While there is a range of magnet thicknesses, we have chosen our dots to be cubic in shape with 2.0ξ as the length of a side. In our case, the mesoscopic magnetic cubes form a square array whose lattice constant is 6.25ξ . We specify the dipole moment of the magnets by calculating the *positive* flux passing through each unit cell. Given in units of the fundamental flux quantum, this quantity provides a natural measure of the dot dipole strength.

In solving the Ginzburg-Landau equations for our geometry, we have replaced continuum variables with their discrete versions on a mesh fine enough to ensure convergence with respect to the discretization (to achieve this, we allow at least 5 grid points per coherence length). Our scheme of discretization is a gauge theoretic formalism (discrete versions of the standard continuum gauge symmetries are imposed) where currents and vector potentials A_{ij}^x and A_{ij}^y occupy the lattice bonds, while order parameter values ψ_{ij} reside on lattice nodes. **Additional details on the discretization scheme can be found in another work [18].** We treat the mesoscopic magnetic dots as square loops of current with a thickness equal to the width of the dot base; the magnetic field and vector potential generated by the magnetic dipoles are then easily calculated. Though we handle the x and y (in-plane coordinates) discretely, the z direction is treated exactly, in the continuum limit.

Via a conjugate-gradient technique, we solve the Ginzburg-Landau equations in an iterative manner. In this method, one first linearizes the Ginzburg-Landau equations about an initial guess. The solution obtained by solving the resulting linear equations is then used as

an input for the next iteration. We simulate in our calculation an experiment in which the effective magnetic dot strengths are varied continuously (to realize this in the laboratory, one could as noted above apply an in-plane magnetic field to tilt the dipole moments of the dot magnets, thereby varying their effective strength). In “rightward sweeps”, we slowly increase the dipole strength. Sweeps range from dipoles too weak to generate any vortex-antivortex pairs to magnetic dots strong enough to destroy the superconductivity altogether. In a rightward sweep (toward stronger dipoles), the results of each calculation are used as the initial guess of the next calculation, in which the Ginzburg-Landau equations are solved for slightly stronger magnetic dots. “Leftward” sweeps are conducted in a very similar way, with each successive calculation using weaker dipoles than the previous one. The sweeps in opposite directions complement each other by highlighting hysteresis effects, thereby revealing which transitions are first order.

To illustrate the configurations which correspond to the phases shown in Fig. 2, we display Cooper pair densities in Fig. 3 and Fig. 4. Vortices and antivortices are readily identified as regions of depleted Cooper pairs. Exploiting the fact that the order parameter phase **has a nonvanishing winding number** at the vortex cores makes it possible to **locate vortices and antivortices**; the line integral $\oint \vec{\nabla}\phi \cdot d\vec{s}$ with the integration contour taken to be a single square of our grid yields $+2\pi$ (-2π) if a (anti) vortex is contained in the square, and is zero otherwise. In terms of currents and magnetic flux, this condition is $\oint \frac{\vec{j}}{|\psi|^2} \cdot d\vec{s} + \Phi_B = \pm 2\pi$ for a vortex or antivortex, respectively. This tool for locating flux quanta permits the precise depiction of vortex configurations, and also conveniently yields ρ_{pair} .

Figure 1 is a plot of ρ_{pair} and the Ginzburg-Landau internal energy for both sweeps to the right and to the left (E_{GL} is given in units of $d\Delta\xi^3$). The discrepancy between opposite sweeps for ρ_{pair} is readily evident. One can also see sudden downward jumps in E_{GL} for both rightward and leftward sweeps. These jumps and the hysteresis effects in ρ_{pair} are a result of the metastability of some of the vortex configurations, signifying that several of the transitions are first order. One can construct a “ground state energy” by selecting the lowest energy from sweeps to the right and to the left, with the preferred state being the vortex configuration corresponding to the lowest energy. In this manner, we have constructed a phase diagram for the system, shown in Fig 2. Figures 3 and 4 depict vortex configurations in salient cases. In the phase diagram, states are classified according to ρ_{pair} , the number of vortex-antivortex pairs. When necessary, as in the case of $\rho_{pair} = 2$, phases are further classified according to the symmetry of the vortex configuration. metastable states are not lowest in energy and are therefore not preferred by the system.

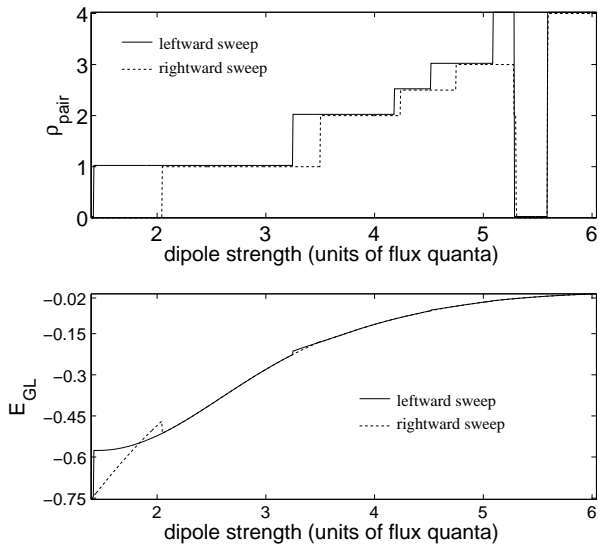


FIG. 1: ρ_{pair} and E_{GL} plots for sweeps to the left and to the right. The energy is given in units of $d\xi^3\Delta$, where Δ is the condensation energy per unit volume and d is the film thickness.

In discussing the phase diagram of Fig. 2, we begin from the left (weak dipoles) and move to the right (toward stronger dipoles). The formation of vortex-antivortex pairs is energetically unfavorable for weak dipoles and, hence, $\rho_{pair} = 0$ for the leftmost state. The next configuration corresponds to a single vortex-antivortex pair per unit cell with vortices in the vicinity of the dot centers and antivortices centrally located in the interstitial areas. With stronger dipoles, there is a first order transition to a configuration for which $\rho_{pair} = 2$. As can be seen in Fig. 3(a), antivortices (small dark regions) are connected with the dot magnets by lobes of depleted Cooper pair density (light areas). These molecule-like complexes are aligned along the unit cell diagonals, thereby breaking $\pi/2$ orientational symmetry. As the dipole strengths are increased further, one finds a state which breaks both orientational and mirror symmetries [see Fig. 3(b)]. As the sudden symmetry breaking suggests, the transition is first order.

Even higher dipole strengths lead to a fractional state, for which $\rho_{pair} = 2.5$. Figs. 3(b) and 3(c) reveal that the transition into this state is a gradual one. Ultimately mirror symmetry is restored, as seen in Fig. 3(c). As one continues the rightward sweep, one encounters a first order transition to a $\rho_{pair} = 3$ state [depicted in Fig. 3(d)]. Again, in view of the significant dissimilarities between the states, this is not surprising. For even larger magnetic dot strengths, the vortex pair density exhibits a surprising nonmonotonicity by jumping suddenly to zero. Despite the abrupt change in ρ_{pair} , the shift to the $\rho_{pair} = 0$ state occurs continuously, through the sequence shown

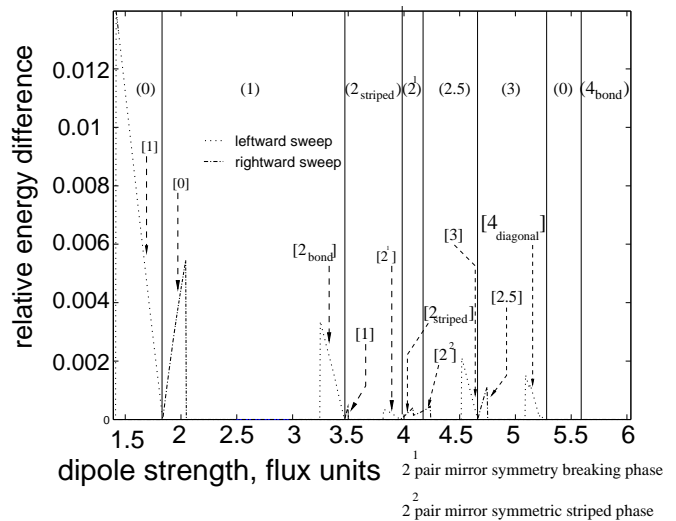


FIG. 2: Phase diagram with metastable states. Stable states indicated by numbers in parenthesis; metastable states by numbers in brackets. These numbers indicate how many vortex-antivortex pairs per unit cell. Dotted (broken) lines indicate energies of metastable states for leftward (rightward) sweeps. “Bond” subscripts indicate states in which antivortices lie along nearest neighbor bonds; “striped” and “diagonal” subscripts indicate antivortices which lie on diagonals (next-nearest neighbor bonds).

in Fig. 4. First, the antivortices rearrange to form the $\rho_{pair} = 3$ configuration depicted in Fig. 4(a). Next, the antivortices are pulled inward, forming the state shown in Fig. 4(b). The triangular structures in Fig. 4(b), each of which contains three vortex-antivortex pairs, then begin to transform. The vortices move outward from the dots to meet the antivortices, which move inward. Ultimately, the flux quantum pairs annihilate and the result is the $\rho_{pair} = 0$ configuration shown in Fig. 4(c). The final transition, one which also occurs in a continuous manner, is to the $\rho_{pair} = 4$ configuration shown in Fig. 4(d). In each unit cell four vortex-antivortex pairs form along nearest neighbor bonds. As the magnetic dipoles are made stronger, the pair separations increase, until the magnetic dipoles become so strong that the superconductivity in the thin film is lost.

This complicated evolution is driven by the competition between intra and interdot potentials for the antivortices. Evidently, for very strong dipoles, the antivortices feel not just the effects of a single magnet, but are affected by neighboring magnets as well, and the state **ultimately** deforms in such a way that the vortices instead reside on nearest neighbor bonds. **The annihilation of flux pairs and the formation of the intermediate $\rho_{pair} = 0$ state is due to the strong suppression of the order parameter in the region surrounding the dots, eliminating energetically costly currents and hence the need for flux quanta.** With

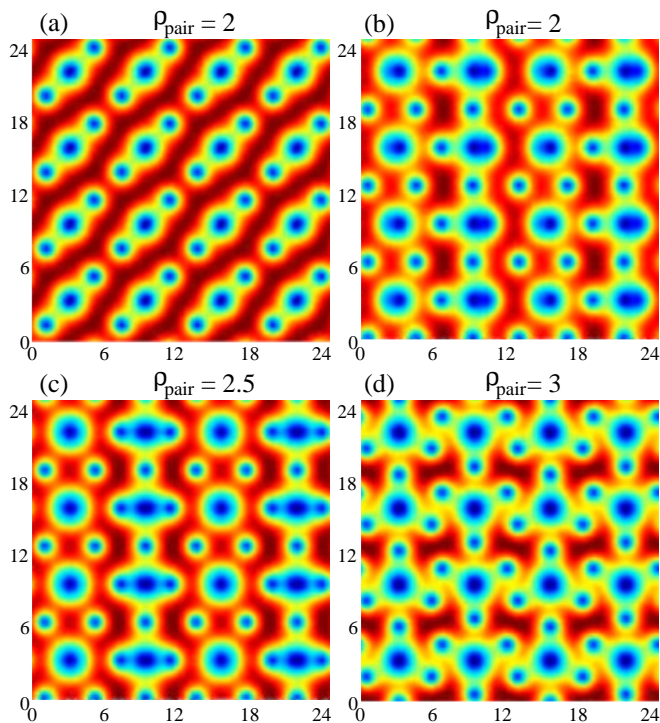


FIG. 3: Cooper pair density plots of stable phases. the images in panels (a), (b), (c), and (d) correspond to dot magnet strengths of 3.61, 4.07, 4.33, and 4.95 fundamental flux units, respectively. **Cooper pair density is highest in red areas and lowest in blue regions.** Antivortices appear as small blue spots, while the large blue spots indicate dot regions.

stronger dipoles, the energy of the state may be lowered by having vortices from neighboring dots share regions of suppressed order parameter along nearest neighbor bonds, leading to the $\rho_{pair} = 4$ configuration. Interestingly, this creates squares of depleted order parameter rotated by 90° relative to the dots themselves.

Conclusions and possibilities for experiment– We have found, even in the absence of any applied magnetic flux, that mesoscopic arrays of magnetic dots can exhibit non-trivial vortex phenomena, including configurations which break lattice symmetries, states with superlattice structure, and a fractional vortex configuration. To realize these states in the laboratory, we have proposed an experiment in which one may vary the effective strength of the dot magnets by using an in-plane magnetic field to tilt the dipole moment. In this way it should be possible to carry out the previously discussed sweeps in magnet strength, making it feasible to access experimentally the stable configurations shown in the phase diagram of Fig. 2 and even some of the states which we have classified as metastable.

Finally, we mention some possible experimental tests for the novel vortex phenomena discussed in this work.

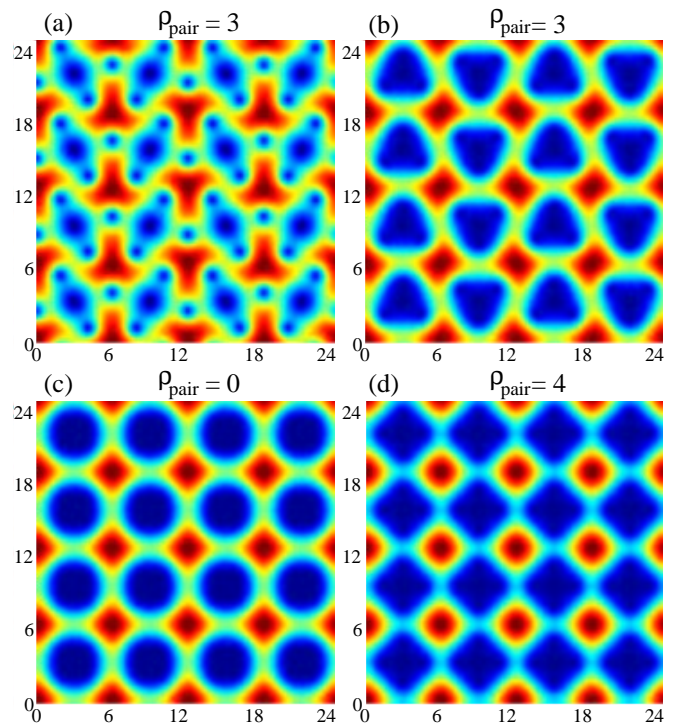


FIG. 4: Cooper pair density plots of stable phases. Images in panels (a), (b), (c), and (d) correspond to magnetic dot strengths equal to 5.16, 5.26, 5.42, and 6.04 fundamental flux units, respectively.

Critical currents are a useful probe; different j_c^x and j_c^y values would signal broken orientational symmetry. The existence of states that break the spatial symmetry of the lattice [e.g., Fig. 3(b)] suggests that Ising physics might be observed in this system at finite temperatures in thermodynamic quantities such as the specific heat. It is also interesting to speculate that the non-monotonic vortex density found in the vicinity of the four vortex pair states (Figs. 4) could lead to a peak in the critical current as a function of perpendicular dipole strength. In any case, our calculations strongly suggest that this system offers a rich phenomenology worthy of further theoretical and experimental investigation.

Acknowledgements– The authors would like to thank M.V. Milošević, Chandan Dasgupta, I. Žutić, and S. Das Sarma for useful discussions. This work was supported by NSF Grant No. DMR01-08451.

-
- [1] M. Baert *et al*, Phys. Rev. Lett. **74**, 3269 (1995).
 - [2] J.I. Martín *et al*, Phys. Rev. Lett. **79**, 1929 (1997).
 - [3] M.J. Van Bael *et al*, Phys. Rev. B **59**, 14674 (1999).
 - [4] J.I. Martín *et al*, Phys. Rev. Lett. **83**, 1022 (1999).
 - [5] M.J. Van Bael *et al*, Physica C, **332**, 12 (2000).
 - [6] M. Lange, *et al*, Euro-phys. Lett. **53**, 646 (2001).

- [7] Martin Lange *et al*, Phys. Rev. Lett. **90**, 197006 (2003).
- [8] I.K. Marmoros, *et al*, Phys. Rev. B **53**, 2677 (1996).
- [9] M.V. Milošević *et al*, Phys. Rev. B **66**, 174519 (2002).
- [10] M.V. Milošević *et al*, Phys. Rev. B **68**, 024509 (2003).
- [11] Valery Prokovsky *et al*, Phys. Rev. Lett. **81**, 2344 (1998).
- [12] Sa-Lin Cheng *et al*, Phys. Rev. B **65**, 024503 (2001).
- [13] R. Šášik *et al*, cond-mat/0003462.
- [14] Serkan Erdin *et al*, Phys. Rev. Lett. **88**, 017001 (2002).
- [15] Serkan Erdin *et al*, Phys. Rev. B **66**, 014414 (2002).
- [16] Serkan Erdin, cond-mat/0211117.
- [17] Gilson Carneiro, cond-mat/0308574.
- [18] D. J. Priour *et al*, Phys. Rev. B **67**, 054504 (2003).